Asian Journal of Chemistry; Vol. 24, No. 2 (2012), 635-640

ASIAN JOURNAL OF CHEMISTRY

www.asianjournalofchemistry.co.in

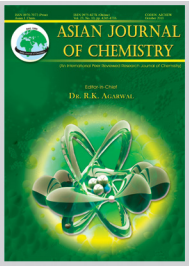

Characterization of Host-Guest Composite Material (SBA-15)-(*p*-Acetylarsenazo)

YU XUE, XIAO-YU FAN and QING-ZHOU ZHAI*

Research Center for Nanotechnology, Changchun University of Science and Technology, 7186 Weixing Road, Changchun 130022, P.R. China

*Corresponding author: Fax: +86 431 85383815; Tel: +86 431 85583118; E-mail: zhaiqingzhou@163.com; zhaiqingzhou@hotmail.com

(*Received*: 3 February 2011; *Accepted*: 12 October 2011) AJC-10496

SBA-15 molecular sieve was synthesized using tetraethylorthosilicate as silica resource in acidic medium by using triblock copolymers ($EG_{20}PG_{40}EG_{20}$) as template. Guest material *p*-acetylarsenazo (ASA*p*A) was incorporated into the molecular sieve host to obtain host-guest composite material (SBA-15)-ASA*p*A. Powder X-ray diffraction results suggested that the ordered degrees of the SBA-15 in the host-guest composite materials were still remained good and the frameworks of the molecular sieves were not destroyed by incorporation of the guest. Infrared spectra showed that frameworks of the host of prepared materials were kept intact. Low-temperature nitrogen adsorption-desorption results at 77 K showed that the surface area and the pore volume of the prepared host-guest composite materials decreased compared to those of the host molecular sieve, indicating that the guest has partially occupied channels of the molecular sieve. Scanning electron microscopic studies indicated that the composite materials (SBA-15)-ASA*p*A presented fibrous appearance and their size was 335 ± 10 and 343 ± 10 nm, respectively. Luminous spectra showed that the prepared host-guest nanocomposite materials have the character of luminescence.

Key Words: *p*-Acetylarsenazo, SBA-15, Host-guest nanocomposite material.

INTRODUCTION

Since 1992, the scientists in the American Mobil Oil Company successfully synthesized MCM-41 mesoporous molecular sieve, the study of mesoporous molecular sieve has drawn international attention of the relevant academic communities. However, because of its poor hydrothermal stability and narrow pore, applications of MCM-41 have been greatly hindered. Zhao *et al.*[1], successfully synthesized SBA-15 mesoporous molecular sieve with larger pore diameter by adopting the method of surfactants. It has the hexagonal pore of high ordering, micropores connecting between pores. By changing the synthesis conditions, the adjustable 4.6 to 30 nm of the pore size can be realized with the thickness of pore wall of 3.1 to 6.0 nm. The mesoporous molecular sieve also has high mechanical strength, good hydrothermal stability (the thermal stability exceeds 900 ºC), long service life and biologically non-toxicity. In the fields such as biology[2], opto-electronics[3], catalysis[4,5], nanomaterials preparation[6], *etc.*, it has shown great potential for applications. In recent years, mesoporous materials have been applied to the optical field. SBA-15 is taken as a main material and certain guest materials are assembled into it, obtaining host-guest nanocomposite materials with light-emitting property[7]. Hoffmann *et al.*[8], on the other way, attached Kr to SBA-15 molecular sieve pores, obtaining the material of photosensitive film. Gao *et al.*[9], grafted the light-emitting molecules onto the modified SBA-15 molecular sieve, selectively detecting zinc ions by using the principle that zinc ion and light-emitting elements will lead to fluorescence quenching. Metivier *et al.*[10], loaded organic fluorescent silica source to SBA-15, thus obtaining mesoporous materials that can be used to achieve the selective testing of mercury ions in water. Descalzo *et al.*[11] synthesized fluorescent hybrid mesoporous materials of through post-processing method and this made good progress of the detection of long-chain carboxylic acids in water. *p*-Acetylarsenazo is an organic dye, with the color reaction with certain metal ions to produce complex and its antiinterference ability and stability are outstanding. It has been applied to the determination of rare earths metal content[12]. So far, no reports on SBA-15, as the host, assembling ASA*p*A material have been revealed. In this study, SBA-15 molecular sieve was prepared as a composite host, then assembled the guest dye ASA*p*A into nanopores of the molecular sieve. The structure and properties of (SBA-15)-ASA*p*A are characterized by chemical analysis, powder X-ray diffraction, low temperature N_2 adsorption-desorption at 77 K, scanning electron microscopy, transmission electron microscopy and luminescent spectra. The results showed that the preparation of the host-guest nanocomposite was very successful, accompanying by the existence of the luminous

property that is not involved in the host or guest. This promises potential application in luminescent materials field.

EXPERIMENTAL

Biparental triblock copolymers, (1,2-ethylene glycol)-block-poly (propyleneglycol)-block-poly(1,2-ethylene glycol) (Fluka, Switzerland); tetraethylorthosilicate (TEOS, AR, Shanghai Chemical Pharmaceutical Co. Ltd., China); *p*-acetylarsenazo (ASA*p*A) (Changke Institute of Chemical Reagents, Jinsheng Chemical Corp.. Ltd., China); deionized water.

Determination of silica in molecular sieves was made by molybdosilicate bule photometry[13]. The content of dye ASA*p*A was obtained by difference. The XRD spectrogram was detected by D5005 diffractometer (Germany Siemens Company). The data of N_2 adsorption/desorptions at low temperature of 77 K were obtained by Micromeritics ASAP2010M (American Mike Company). Scanning electron microscopy study was made by adopting Japanese JEOL JSM-5600L scanning electron microscope. Transmission electron microscopic images were recorded by adopting Japanese JEOL 2010 transmission electron microscope. Luminescence spectra were recorded at room temperature (20 ºC) on the SPEX-FL-2T-2 double-grating fluorescence spectrometer (SPEX Company, USA).

Preparation of SBA-15 mesoporous molecular sieve: First, 2 g of biparental triblock copolymers (1,2-ethylene glycol)-block-poly(propylene glycol)-block-poly (1,2-ethylene glycol) (average molecular weight, 5800) was dissolved in 15 g of deionized water and 60 g of 2 mol o L^{-1} hydrochloric acid solution and stirred. Then, 4.25 g of TEOS was slowly dripped into it, forming a homogeneous solution. The best initial molar ratio of each material was: (T: TEOS: HCl: H_2O = 1:59:348: 2417). Then, this mixed solution was stirred for 24 h at 40 ºC and the crystallized solution was put into the reaction vessel with plastic substrates at 100 ºC for 2-day crystallization. Finally, the crystallized product went through filtration and was washed with deionized water, dried at room temperature, placed in a static air at 550 ºC and finally was calcined for 24 h. Then, the triblock copolymer was removed, getting mesoporous silica SBA-15 as white powder[1].

Preparation of host-guest nanocomposite material (SBA-15)-ASA*p*A: The SBA-15 was dehydrated at 200 ºC for 3 h. Two of the above-mentioned SBA-15 (0.300 g for each) were, respectively, placed in 30 mL of aqueous solution of ASA*p*A with the concentration of 5.0×10^{-3} and 5.0×10^{-4} mol/L. They were stirred in 50 mL beakers at room temperature for 48 h. Obtained products were filtered and carefully and repeatedly washed with deionized water until getting colourless filtrate. At 60 ºC, products were placed for arefaction for 6 h. Then host-guest nanocomposite materials (SBA-15)-ASA*p*A were generated. The sample made from the aqueous solution of ASA*p*A of lower concentration (5.0×10^{-4} mol/L) was marked as (SBA-15)-ASA*p*A (I), while the one made from the ASA*p*A aqueous solution of higher concentration (5.0×10^{-3} mol/L) was marked as (SBA-15)-ASA*p*A (II).

RESULTS AND DISCUSSION

Chemical analysis: Determination of silica in the host-guest composite materials (SBA-15)-ASA*p*A was made by molybdosilicate blue photometry[13]. The content of dye ASA*p*A was obtained by difference. The results of chemical analysis show that the contents of dye ASA*p*A in the (SBA-15)-ASA*p*A for (I) and (II) samples are 3.33 and 4.77 %, respectively. This indicates that ASA*p*A existed in the host-guest composite materials (SBA-15)-ASA*p*A.

Powder X-ray diffraction analysis: Fig. 1 shows XRD curves represented for three samples, namely, SBA-15, (SBA-15)-ASApA-(I), (SBA-15)-ASApA-(II) at 0.4-10º, from which one can see that in curve (a), (b) and (c), (100) diffraction peaks of SBA-15 molecular sieve have all emerged with great intensity. Curve (a) even shows three relatively weaker diffraction peaks, corresponding to (110), (200) and (210), which are clearly visible. This shows that the prepared SBA-15 molecular sieve has good quality[1]. In Fig. 1, compared with curve (a), curve (b) contains diffraction peaks of decreased intensity while the diffraction intensity in curve (c) decreases even more, so that diffraction peaks (200) and (210) disappear. This shows that ASA*p*A molecules enter into the pores of molecular sieve, leading to a lowered diffraction contrast between the framework and the pores of SBA-15 molecular sieve. The more ASApA molecules enter, the more impact will be formed on the pore structure.

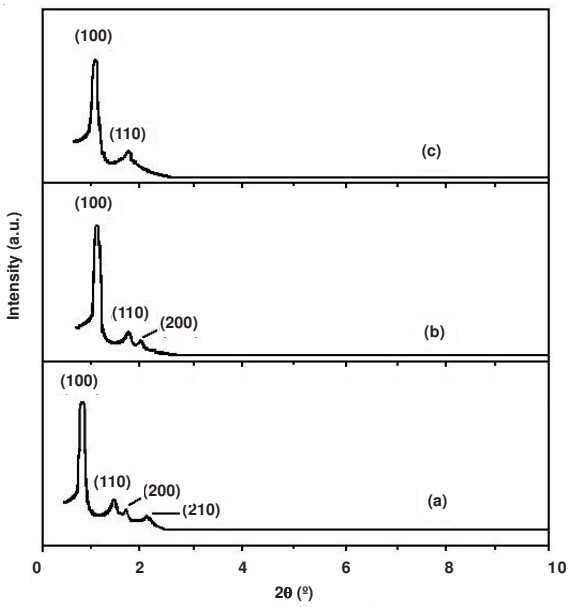

Fig. 1. XRD patterns of the samples: (a) SBA-15; (b) (SBA-15)-ASA*p*A (I); (c) (SBA-15)-ASA*p*A (II)

Low temperature N_2 adsorption-desorption isotherm at 77 K: Figs. 2 and 3 show the N_2 adsorption-desorption isotherms and pore size distribution curves at the low temperature of 77 K corresponding to samples SBA-15, (SBA-15)-ASA*p*A (I) and (SBA-15)-ASA*p*A (II), respectively. Usually specific pressure (relative pressure) p/p_0 is used to represent pressure; p is the real pressure of the gas; p_0 is the saturated vapour pressure when the gas is in the measurement of temperature. Adsorption equilibrium isotherm can be divided into two parts, namely, adsorption and desorption. The shape of adsorption equilibrium isotherms is related to the structure of pore materials. Fig. 2 shows that N_2 adsorption-desorption isotherms of three samples belong to the Langmuir IV type and have the hysteresis

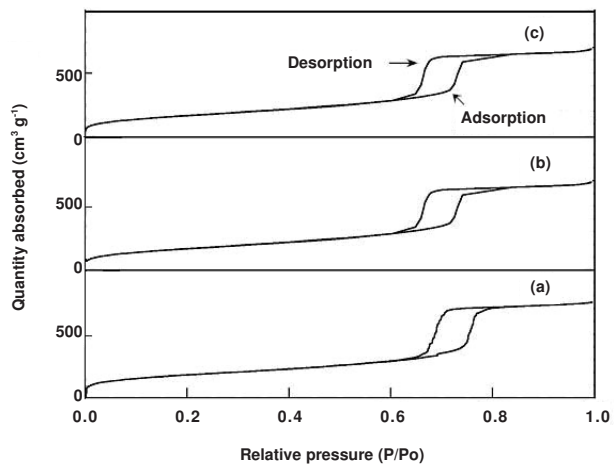

Fig. 2. Low temperature N_2 adsorption-desorption curves: (a) SBA-15; (b) (SBA-15)-ASA*p*A (I) ;(c) (SBA-15)-ASA*p*A (II)

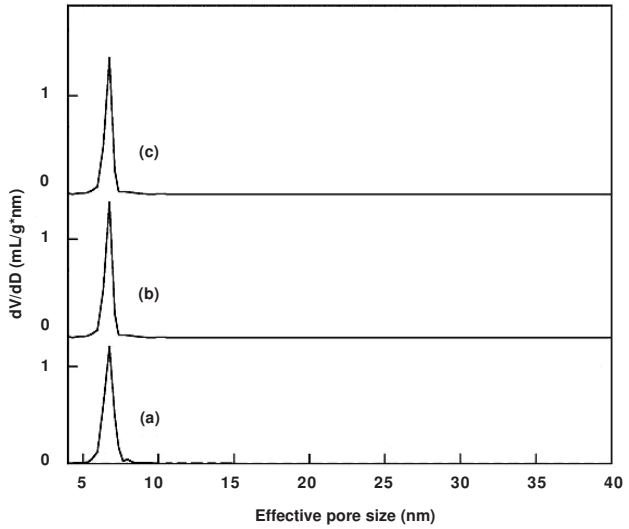

Fig. 3. Pore size distribution patterns: (a) SBA-15; (b) (SBA-15)-ASA*p*A (I); (c) (SBA-15)-ASA*p*A (II)

loop of H1 type. It can be proved that they have a typical characteristic of mesoporous materials with one-dimensional cylindrical pores. Typical mesoporous materials have single pore size distribution, whose adsorption of nitrogen at low temperature can be divided into three phases. The first phase provides smaller pressure and nitrogen molecules are adsorbed on pores in monolayer, which makes the absorption curve flattening. The second stage provides the medium pressure range. Due to the capillary cohesion of nitrogen molecules adsorbed on pores in monolayer and multilayer adsorption, the adsorption capacity increases rapidly with increased pressure. In third stage, the adsorption gradually reaches saturation so that adsorption capacity slowly increases with increasing pressure. The more the sudden jump pressure occurs in the medium pressure range, the larger the sample aperture is. On the other hand, in the phase of sudden jump, the steep degree of the curve can be used to measure whether the sample aperture is uniform. The large rangeability (large slope) represents good pore uniformity, *i.e.*, pore size distribution is narrow.

Fig. 2 shows that at low temperature, N_2 adsorption-desorption isotherms of SBA-15, (SBA-15)-ASA*p*A (I) and (SBA-15)-ASA*p*A (II) belong to the same type, indicating that the introduction of ASA*p*A does not destroy the SBA-15 mesoporous pore structure. From the perspective of branches of adsorption and desorption, three samples have generated three phases, very consistent with the adsorption characteristics of mesoporous materials. First of all, when the relative partial pressure changes from 0.60 to 0.62, the adsorption curve is more gentle and then N_2 adsorption-desorption curve emerges into sudden jump when relative partial pressure enters a medium-pressure zone of 0.80-0.82 with a great slope. This indicates the samples have uniform and regular pore structure and finally, increasing adsorption capacity tends to be gentle when the relative partial pressure between 0.82 to 1.00 increases with increasing relative pressure, indicating that the sample adsorption gradually reaches saturation. Compared with non-assembled SBA-15, samples (SBA-15)-ASA*p*A (I) and (SBA-15)-ASA*p*A (II) have a relatively smaller sudden jump range of the relative partial pressure. That is because ASA*p*A is assembled into the pores of the molecular sieve, making the pore diameter smaller. Fig. 3 shows the pore size distribution curves of the samples SBA-15, (SBA-15)-ASApA (I) and (SBA-15)-ASA*p*A (II), indicating that the pore sizes of (SBA-15)-ASA*p*A (I) and (SBA-15)-ASA*p*A (II) have been reduced compared with that of the non-assembled samples SBA-15. This is in line with the reducing pressure range of breaking pressure of samples (SBA-15)-ASA*p*A (I) and (SBA-15)-ASA*p*A (II) in Fig. 2.

When integrated with XRD diagram of samples in Figs. 2 and 3, structural parameters can be calculated and shown in Table-1. Data in Table-1 show that the sample (SBA-15)-ASApA (I), compared with SBA-15, has lower parameters of surface area, pore size, pore volume while the (SBA-15)-ASA*p*A (II) with higher ASA*p*A level is reduced more significantly because ASA*p*A is assembled into the molecular sieve and occupies its pores. In addition, pore walls of (SBA-15)-ASA*p*A (I) and (SBA-15)-ASA*p*A (II) have increased compared with that of SBA-15, because ASA*p*A has occupied the inner surface of pore walls and adsorbed on them, thickening those pore walls, which also proves ASA*p*A has been successfully assembled into the pores of the molecular sieve. In the composite materials, ASA*p*A molecules mainly combined with the inner surface of pores by Vander Waals' force.

To further study the host-guest nano-composite materials, we use the normalized surface area for quantitative calculation according to Table-1 in order to determine the shapes of guest dye molecules in mesoporous molecular sieve pore. The formula of normalized surface area (NSA) is as follows[14]:

$$NSA = \frac{SA_1}{1-y} \times \frac{1}{SA_2} \quad (1)$$

In the above formula, the mass fraction of guest dye molecules in the composite material is set as y, while SA_1 and SA_2 represent surface area of (SBA-15)-ASA*p*A composite material and nano SBA-15 molecular sieve, respectively. According to calculation results of NSA, guest materials usually have three patterns of distribution.

First of all, when NSA << 1, it shows that the guest materials present as relatively large graininess in the composite.

TABLE-1
PORE STRUCTURE PARAMETERS OF THE SAMPLES

Sample	Crystal face spacing (d_{100}) (Å)	Unit cell parameter (a_0)[a] (Å)	BET surface area (m^2/g)	Pore volume[b] (cm^3/g)	Pore size[c] (Å)	Wall thickness[d] (Å)	Content of ASA*p*A (wt. %)
SBA-15	95.6	110.4	662	1.14	67.7	42.7	0
(SBA-15)-ASA*p*A (I)	105.4	121.7	601	1.01	62.1	59.6	3.33
(SBA-15)-ASA*p*A (II)	116.3	134.3	553	0.89	61.1	73.2	4.77

a: Unit cell parameter, $a_0 = \frac{2}{\sqrt{3}} d_{100}$, b: BJH adsorption cumulative volume of pores, c: Pore size calculated from the adsorption branch, d: Wall thickness calculated by (a_0 - pore size).

Due to the entering of such graininess, molecular sieve generates pore blocking with the performance of a rapidly decreased pore volume, specific surface area and pore size of composite materials in relation to the molecular sieve (Fig. 4).

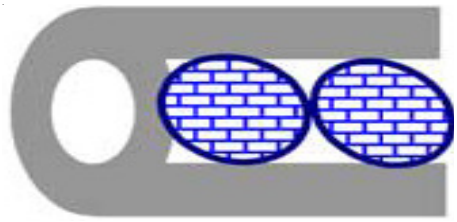

Fig. 4. Guest phase assembly type I in molecular sieve channel

Secondly, when NSA ≈ 1, this shows the guest material has generated an amorphous layer in the pore of host material, which closely covers the inner surface of the pore of molecular sieve (Fig. 5). Since these particles are attaching to inner surface of the pore of molecular sieve, a new surface is formed which only covers the original surface. Therefore, the NSA value of such material is close to 1.

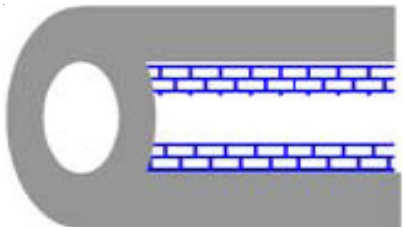

Fig. 5. Guest phase assembly type II in molecular sieve channel

Thirdly, when NSA > 1, this shows the guest material generate very small nano-crystals (Fig. 6). These nano-crystals, scattered over the inner and outer surface of molecular sieve, have smaller nanoparticle sizes than the pore size, so that specific surface area of composite material will not generate clogging pores due to the introduction of guest material. Moreover, the specific surface area will be increased because of it.

Through calculation, NSA value of (SBA-15)-ASApA (II) is 0.94, indicating that the guest dye molecules form an amorphous layer in the pores of SBA-15 molecular sieve (Fig. 5) and closely cover the inner surface of pores of the molecular sieve while NSA value of (SBA-15)-ASA*p*A (I) is 0.88 with higher concentration of ASA*p*A. The reason is because there are more guests entering into the pores of

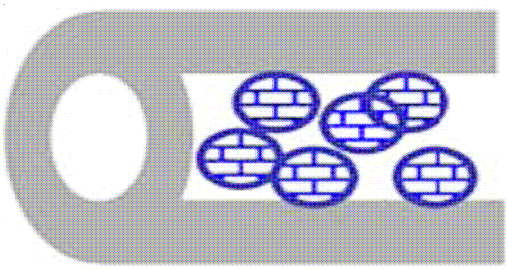

Fig. 6. Guest phase assembly type III in molecular sieve channel

molecular sieve host and blocking pores. This results in lowered specific surface area and pore volume of composite materials, which matches results of the adsorption-desorption experiment.

Scanning and transmission electron microscopic images: Fig. 7 shows the SBA-15 scanning electron microscopic images which shows that the appearance of prepared fibrous molecule is very regular, accompanying by a few globular particles with an average particle size of 333 ± 5 nm. Fig. 8 shows scanning electron microscopic images of (SBA-15)-ASApA (I). Its surface has no glomerated ASA*p*A molecules, whose particle morphology maintains a good state compared with Fig. 7, still presenting a small amount of fibrous and globular particles. However, the degree of order decreases and an average diameter was 335 ± 10 nm, slightly increased as compared with non-assembly state. This is because, the guest is successfully transplanted into the molecular sieve through the liquid dye, causing increased particle size. Fig. 9 is (SBA-15)-ASA*p*A (II) scanning electron microscopic images, shows that its surface has no glomerated ASA*p*A molecules, still presenting a small amount of fibrous and globular particles,

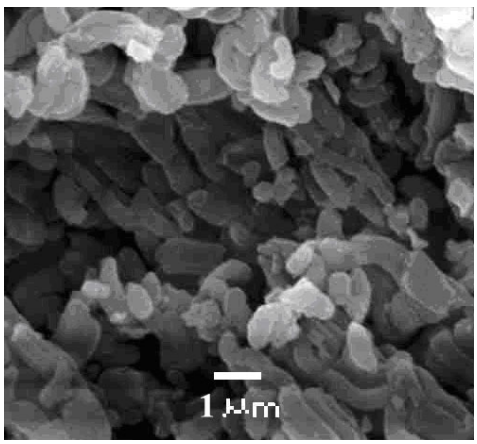

Fig. 7. Scanning electron microscopic images of SBA-15

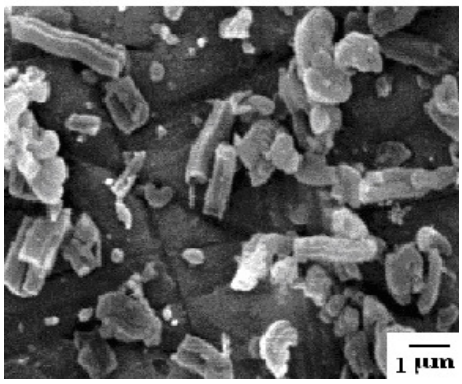

Fig. 8. Scanning electron microscopic images of (SBA-15)- ASA*p*A (I)

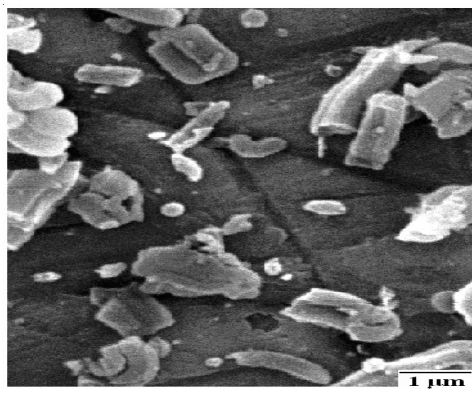

Fig. 9. Scanning electron microscopic images of (SBA-15)- ASA*p*A (II)

but the degree of order decreases and an average diameter was 343 ± 10 nm. Compared with the shape in Fig. 8, it has the same shape, but the average size is increasing. This is because the sample (SBA-15)-ASA*p*A (II) has higher guest dye content than the (SBA-15)-ASA*p*A (I), that is, (SBA-15)-ASA*p*A (II) has more ASA*p*A entering into the channels of molecular sieves, followed by further increases of the sample particle sizes.

Fig. 10 is the transmission electron micrograph of (SBA-15)-ASA*p*A (I), filmed from the vertical direction to the pore. In the figure, it can be seen that the sample has ordered two-dimensional hexagonal pores structure. Molecular sieve framework and the pores are intact and the pore surface has no glomerated ASA*p*A molecules, indicating that the guest dye has been successfully assembled into the internal pores of the molecular sieve. The (SBA-15)-ASA*p*A composite was successfully prepared.

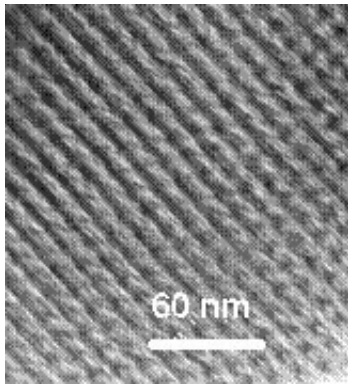

Fig. 10. Transmission electron micrograph of (SBA-15)-ASA*p*A

Luminescent spectra: Fig. 11 is the excitation-emission spectra of the sample (SBA-15)-ASA*p*A (II). As the host material, SBA-15 molecular sieve itself does not have luminosity under normal states, the guest material of ASA*p*A molecule exists in the form of agglomeration. Therefore, the interaction of molecular vibration is strong and the vibration relaxation influence is great, leading to the inferior position in the competition of inactivation process of radiative transition and the vibration relaxation. This reduces remarkably the chances of producing fluorescence. From Fig. 11, it can be seen that the emission wavelength of the host-guest nanocom-posite (SBA-15)-ASA*p*A is 467 nm, obtaining a luminescent property that does not exist in the host and the guest. Light-emitting of (SBA-15)-ASA*p*A consists of two main factors, first of all, highly ordered nanopores of the host SBA-15 molecular sieve constrain the guest dye molecules. When the guest molecules enter into the nanopores, interactions between molecules are significantly diminished. The risk of dissipating energy through the vibration relaxation of excited molecules is significantly reduced, thus enhancing the radiative transition. In addition, the inner surface of the host molecular sieve has a large number of hydroxyl and the guest dye molecules in the host pores of molecular sieve can create bond with some of the hydroxyl, which can increase the rigidity of the structure of guest dye molecules to improve the efficiency of its own fluorescence. When the host material gains excitation energy, the guest dye molecules can also improve the efficiency of gaining excited energy through main bonds with the host so as to enhance the radiative transition and increase fluorescence intensity.

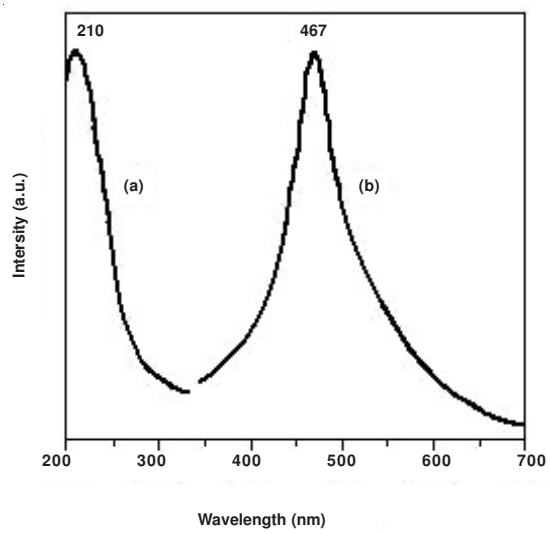

Fig. 11. Luminescent spectra of (SBA-15)-ASA*p*A: (a) excitation spectrum; (b) emission spectrum

Conclusion

In this work, the host-guest nanocomposite materials (SBA-15)-ASA*p*A were successfully prepared. Through powder XRD, low temperature N_2 adsorption-desorption, scanning and transmission electron microscopy and luminescence spectra, the (SBA-15)-ASA*p*A samples were characterized. The characterized results showed that the preparation of (SBA-15)-

ASA*p*A host-guest nanocomposite materials was very successful and the guest material was assembled into the pores of the host molecular sieve. The (SBA-15)-ASA*p*A host-guest composite materials have luminosity at 467 nm. They have application in the field of luminous materials.

REFERENCES

1. D.Y. Zhao, J.L. Feng, Q.S. Huo, N. Melosh, G. H.Fredrickson, B.F. Chmelka and G.D. Stucky, *Science*, **279**, 548 (1998).
2. Y.C. Dong, T. Qi, Y.C. Qin, L.N. Wang, J.G. Li and Y. Zhang, *Modern Food Sci. Technol*., **23**, 19 (2007).
3. Y.J. Yang, L. Zhang, Y. Xu, D. Wu, Y.H. Sun, S.N. Zhao, H.J. Wang, H.B. Lu and X.D. Jiang, *High Power Laser and Particle Beams*, **20**, 935 (2008).
4. M. Hartmann, *Chem. Mater*., **17**, 4577 (2005).
5. M. Miyahara, A.Vinu, K. Z.Hossain, T. Nakanishi and K. Ariga, *Thin Solid Films*, **499**, 13 (2006).
6. Y. Zhou, G.H. Yu, Y. Zhang, J.N. Li and Y.S. Qiu, *New Carbon Mater*., **23**, 63 (2008).
7. S.Z. Wang, D.G. Choi and S.M. Yang, *Adv. Mater*., **14**, 1311 (2002).
8. T. Hofmann, D. Wallacher, P. Huber, R. Birringer, K. Knorr, A. Schreiber and G.H. Findenegg, *Phys. Rev. B*, **72**, 4122 (2005).
9. L. Gao, Y. Wang, J.Q. Wang, L. Huang, L. Shi, X. X. Fan, Z.G. Zou, T. Yu, M. Zhu and Z.S. Li, *Inorg. Chem*., **45**, 6844 (2006).
10. R. Metivier, I. Leray, B. Lebeau and B. Valeur, *J. Mater. Chem*., **15**, 2965 (2005).
11. A.B. Descalzo, K. Rurack, H. Weisshoff and R. Martfnez-Mafiez, *J. Am. Chem. Soc*., **127**, 184 (2005).
12. J.M. Pan, Z.J. Li, Q.Y. Zhang and G.Z. Fan, New Chromogenic Reagents and their Application in Spectrophotometry, Beijing: Chemical Industry Press, p. 54 (2003).
13. Q.Z. Zhai and Y.C. Kim, *Chin. J. Spectrosc. Lab*., **15**, 82 (1998).
14. L. Vradman, M.V. Landau, D. Kantorovich, Y. Koltypin and A. Gedanken, *Micropor. Mesopor. Mater*., **79**, 307 (2005).